Auxiliary material for paper 2010GL043918.

Detecting low-frequency earthquakes within non-volcanic tremor in Southern Taiwan triggered by the 2005 Mw8.6 Nias earthquake

Chi-Chia Tang[1, 2], Zhigang Peng[2], Kevin Chao[2], Chau-Huei Chen[1*], and

Cheng-Horng Lin[3]

1. Institute of Seismology, National Chung Cheng University, 168 University Rd., Min-Hsiung, Chia-Yi County 62102, Taiwan

2. School of Earth and Atmospheric Sciences, Georgia Institute of Technology, 311 Ferst Drive, Atlanta, Georgia 30332, U.S.A.

3. Institute of Earth Sciences, Academia Sinica, 128, Sec. 2, Academia Rd., Nangang, Taipei, 11529, Taiwan

Tang, C.-C., Z. Peng, K. Chao, C.-H. Chen, and C.-H. Lin (2010), Detecting low-frequency earthquakes within non-volcanic tremor in Southern Taiwan triggered by the 2005 Mw8.6 Nias Earthquake, Geophys. Res. Lett., submitted.

Introduction:

This auxiliary material contains 2 tables and 8 figures.

Table S1. *Chen et al.*'s [2001] Model

Layer	Depth (km)	Vp (km/s)	Vp/Vs
1	0~2	4.01	1.78
2	2~5	5.56	1.78
3	5~10	5.96	1.79
4	10~15	6.27	1.83
5	15~25	6.63	1.75
6	25~35	7.06	1.79
7	35~50	7.87	1.77

Table S2. 1-D averaged model from *Wu et al*. [2007] that bounds the initial location of the 10 LFEs: longitude between 120.7°E and 121.0°E and latitude between 22.9°N and 23.3°N.

Layer	Depth (km)	Vp (km/s)	Vp/Vs
1	0~2	3.82	1.74
2	2~4	4.93	1.68
3	4~6	5.51	1.70
4	6~9	5.63	1.70
5	9~13	5.83	1.76
6	13~17	5.99	1.75
7	17~21	6.06	1.75
8	21~25	6.13	1.71
9	25~30	6.25	1.71
10	30~35	6.54	1.73
11	35~50	7.03	1.75

Figure S1

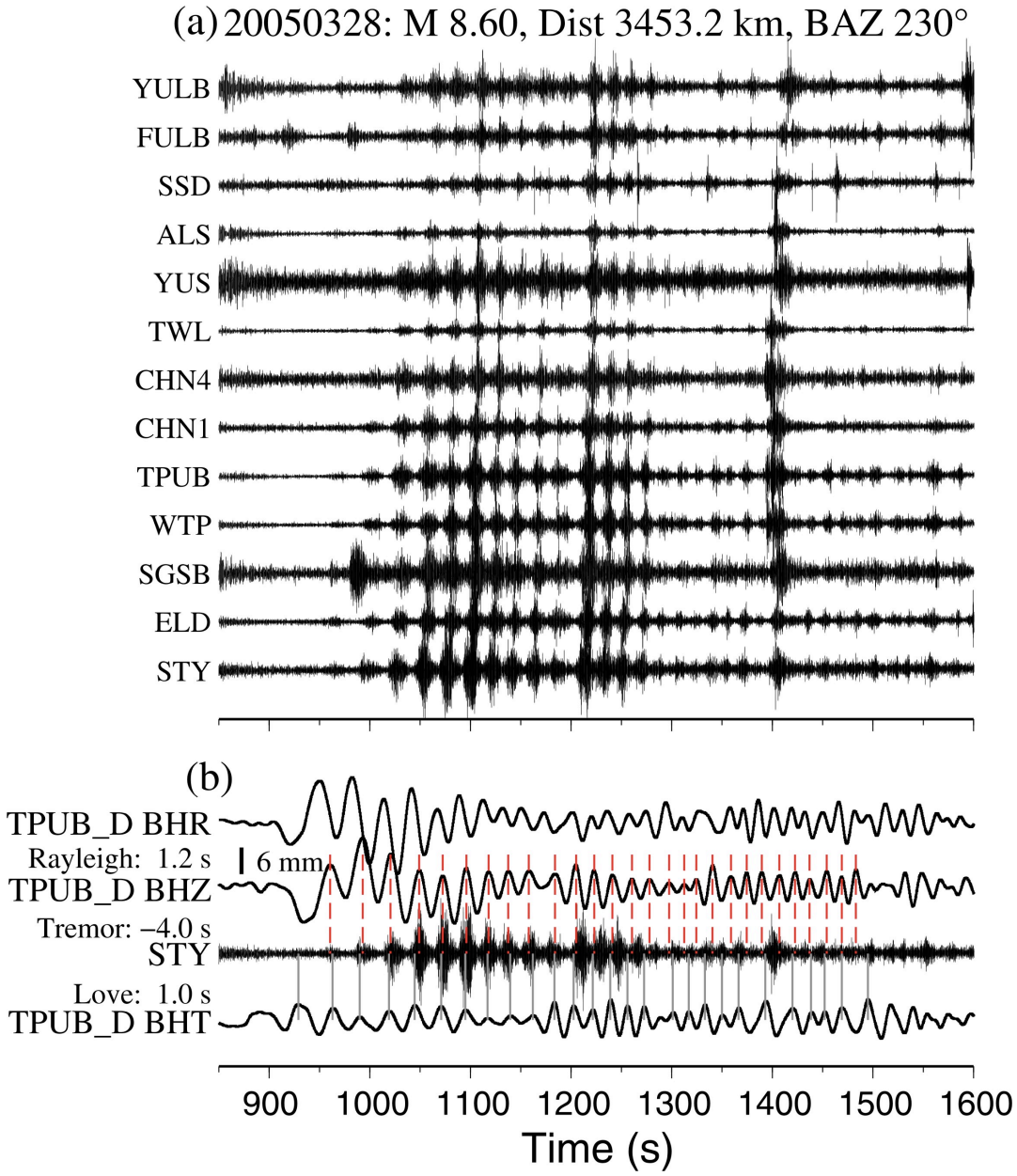

Figure S1. **(a)** The 2-8 Hz band-pass-filtered seismograms in the north component showing tremor triggered by the 2005 Mw8.6 Nias earthquake. The seismograms are plotted from the bottom to top with increasing epicentral distances to the centroid of the 41 LFEs. **(b)** A comparison between the three-component displacement seismograms recorded at the broadband station TPUB and band-pass filtered north-component seismogram at the short-period CWB station STY. The vertical red and gray lines mark the peaks in the vertical and transverse components, respectively. All seismograms have been time-shifted back to the LFE centroid location to reflect the relationship between the surface waves and tremor at the source region. The time is relative to the origin time of the Nias mainshock.

Figure S2.

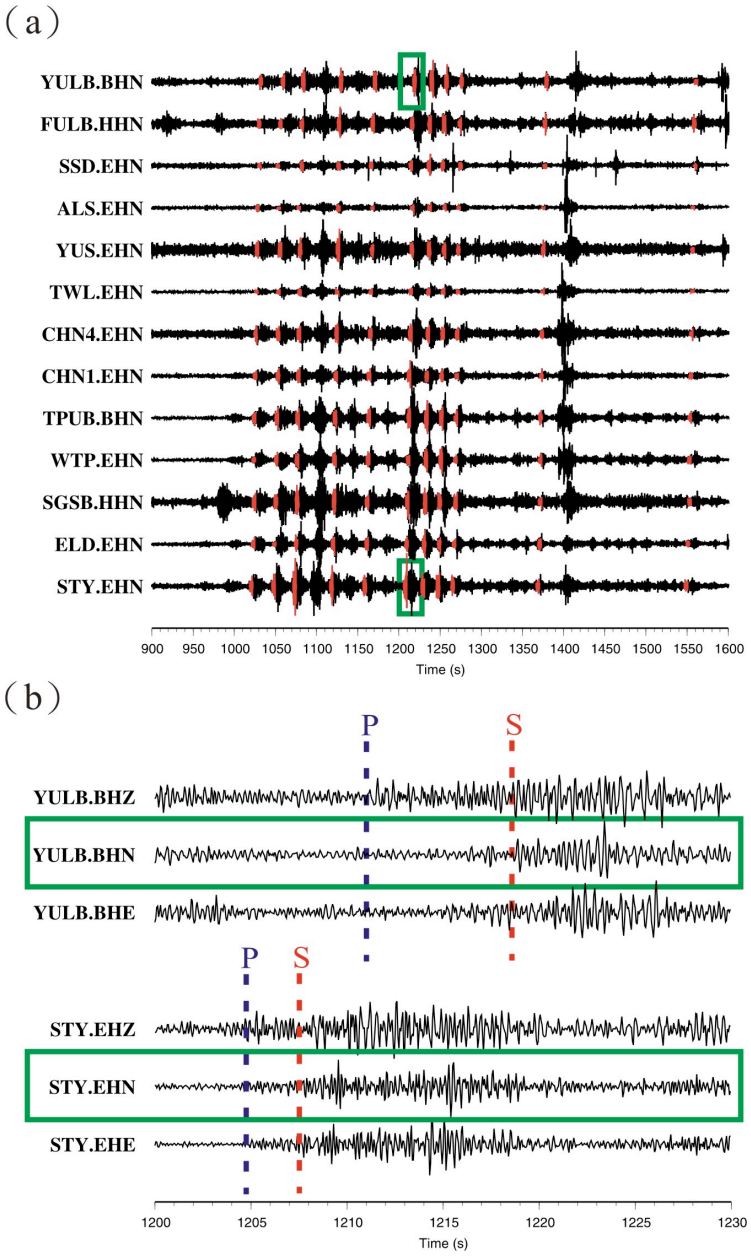

Figure S2. (a) The 2-8 Hz band-pass-filtered north-component seismograms showing triggered tremor for the Nias earthquake. The red segments represent 2 s before and after the predicted *S*-wave arrivals of the 11 templates. Two green squares mark the *S*-wave arrivals for stations YULB and STY. The seismograms are plotted from the bottom to top with increasing epicentral distances to the centroid of the 11 LFEs. **(b)** 3-component seismograms for a LFE recorded at stations YULB and STY. Blue and red dashed lines mark the handpicked *P*- and *S*-wave arrivals, respectively.

Figure S3

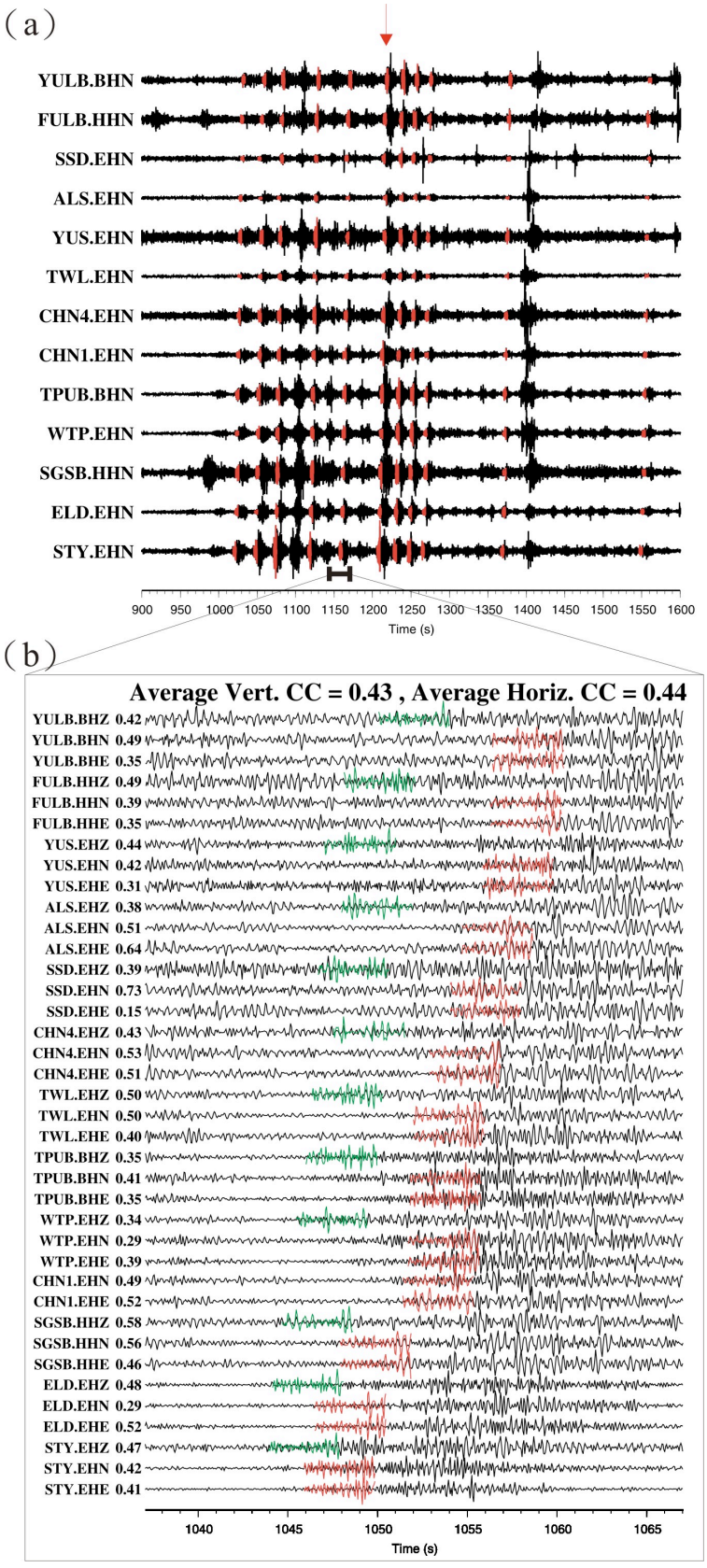

Figure S3. (a) The 2-8 Hz band-pass-filtered north-component seismograms

showing triggered tremor for the Nias earthquake. The red segments represent 2 s before and after theoretical *S*-wave arrivals of the LFEs. The seismograms are plotted from bottom to top with increasing epicentral distances to the centroid of the 41 LFEs. The red arrow indicates the time segment of a template used to detect a new LFE in (b). **(b)** An example showing the waveform detections of *P* (green lines) and *S* (red lines) waves among the initial 11 handpicked events. Individual CC value is shown on the left side and the average CC values for vertical and horizontal component are shown on the top.

Figure S4.

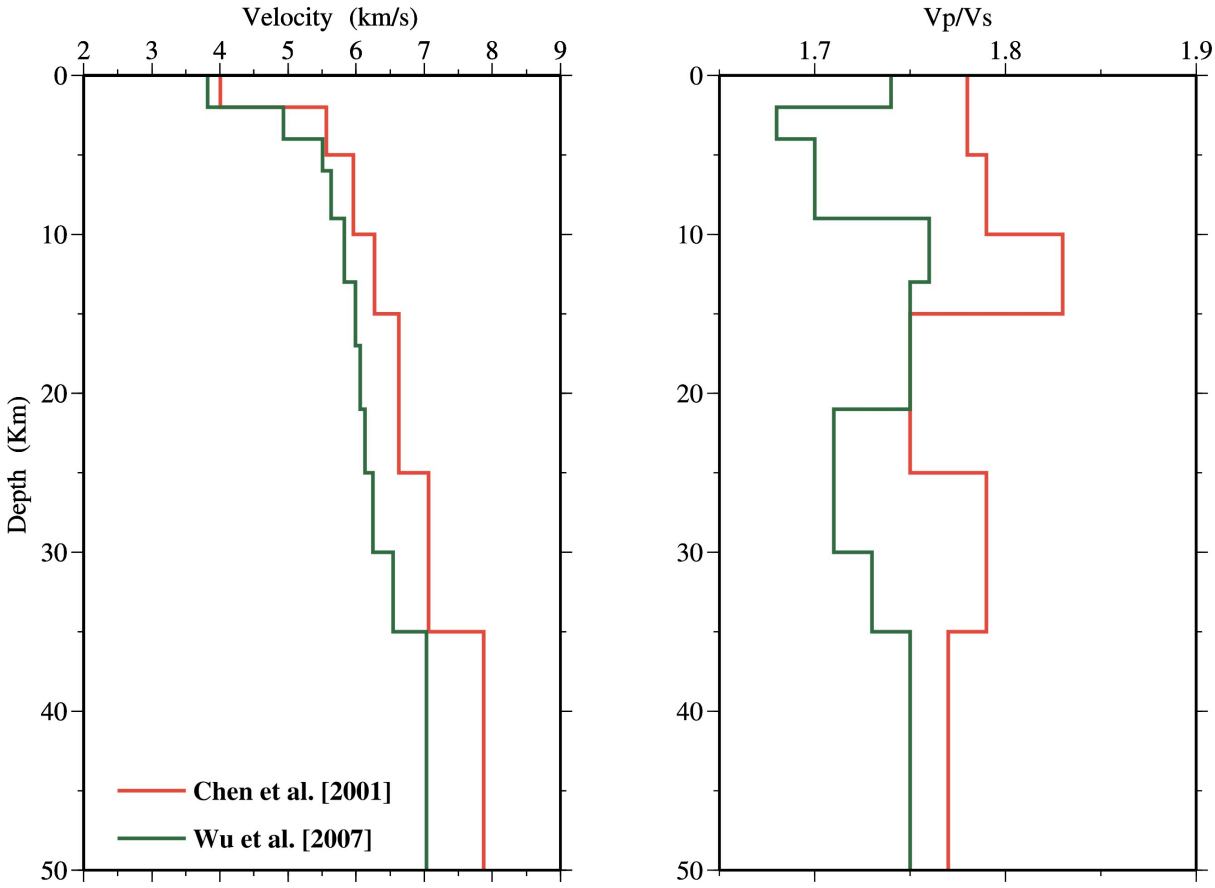

Figure S4. Comparison of the *P*-wave velocities (left) and the Vp/Vs ratios (right) between the 1D velocity model of *Chen et al.*[2001] (red lines) and the 1D velocity model averaged from the 3D velocity model of *Wu et al.*'s [2007] (green lines).

Figure S5.

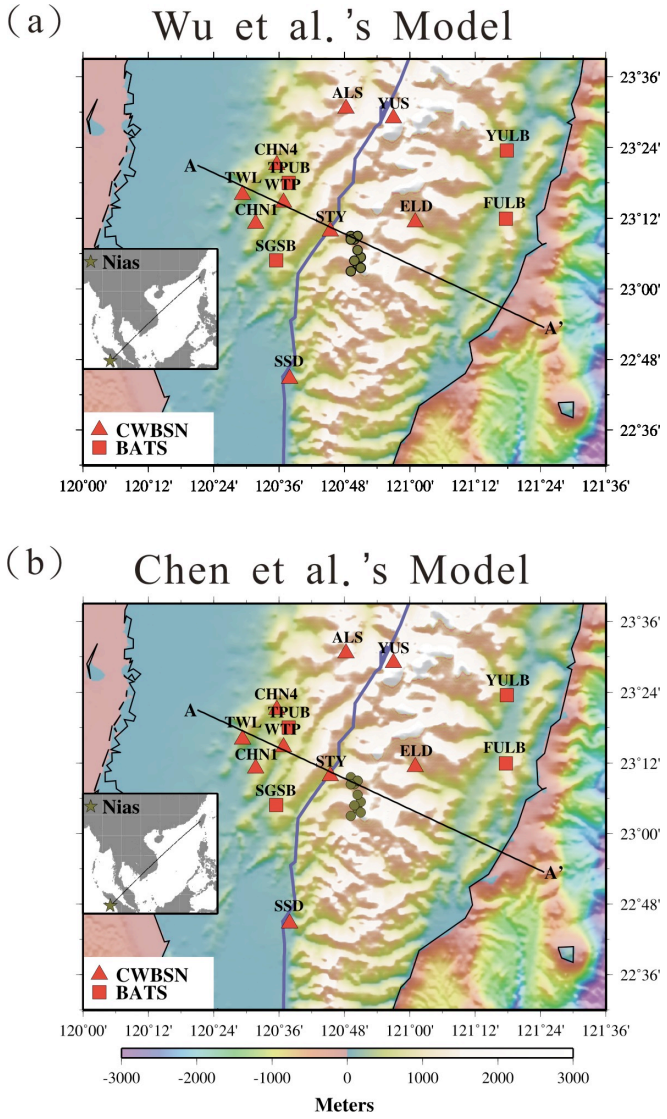

Figure S5. The epicentral locations of the 11 template LFEs according to **(a)** the 1-D average model derived from *Wu et al.*'s [2007] model and **(b)** *Chen et al.*'s [2001] model. Other symbols and notations are the same as in Figure 1a.

Figure S6.

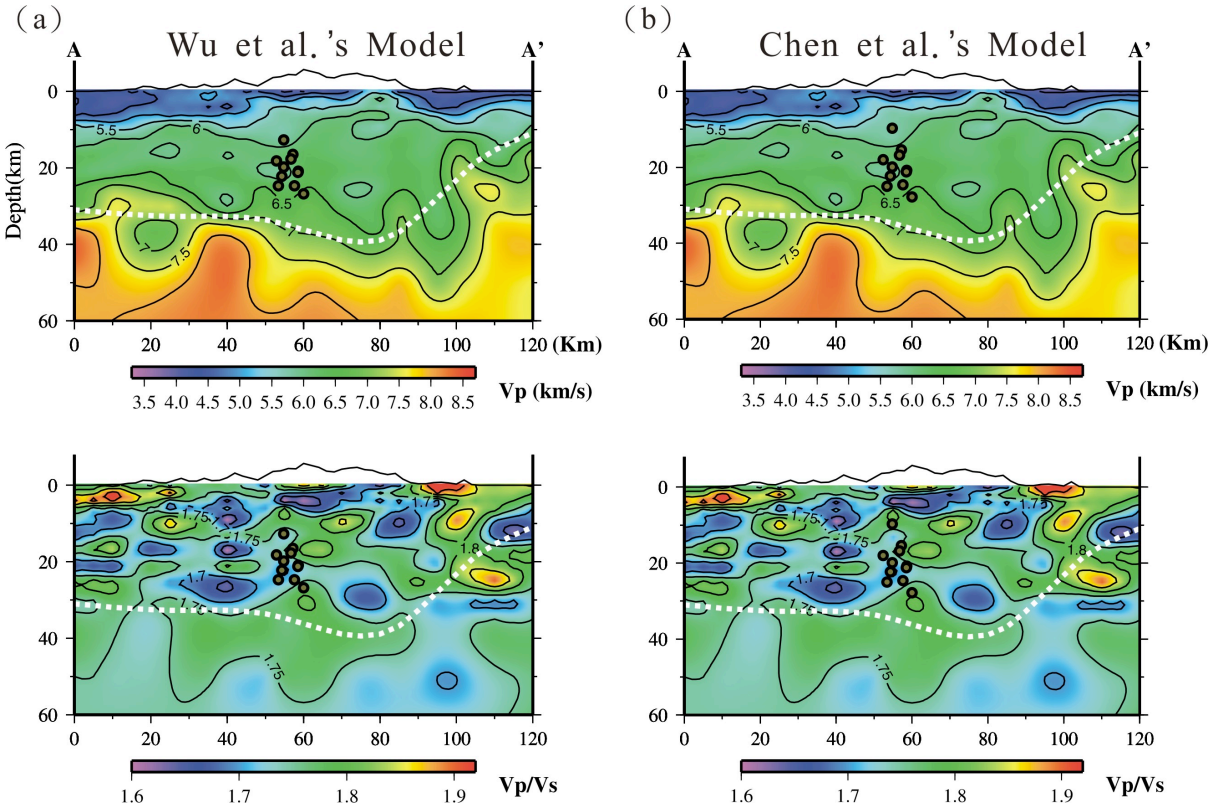

Figure S6. The depth distribution of the 11 template LFEs plotted on top of the Vp (top) and the Vp/Vs models (bottom) of *Wu et al.* [2007]. These events were located according to the 1-D velocity model averaged from **(a)** the *Wu et al.* [2007] 3-D velocity model, and **(b)** the 1-D velocity model of *Chen et al.* [2001].

Figure S7.

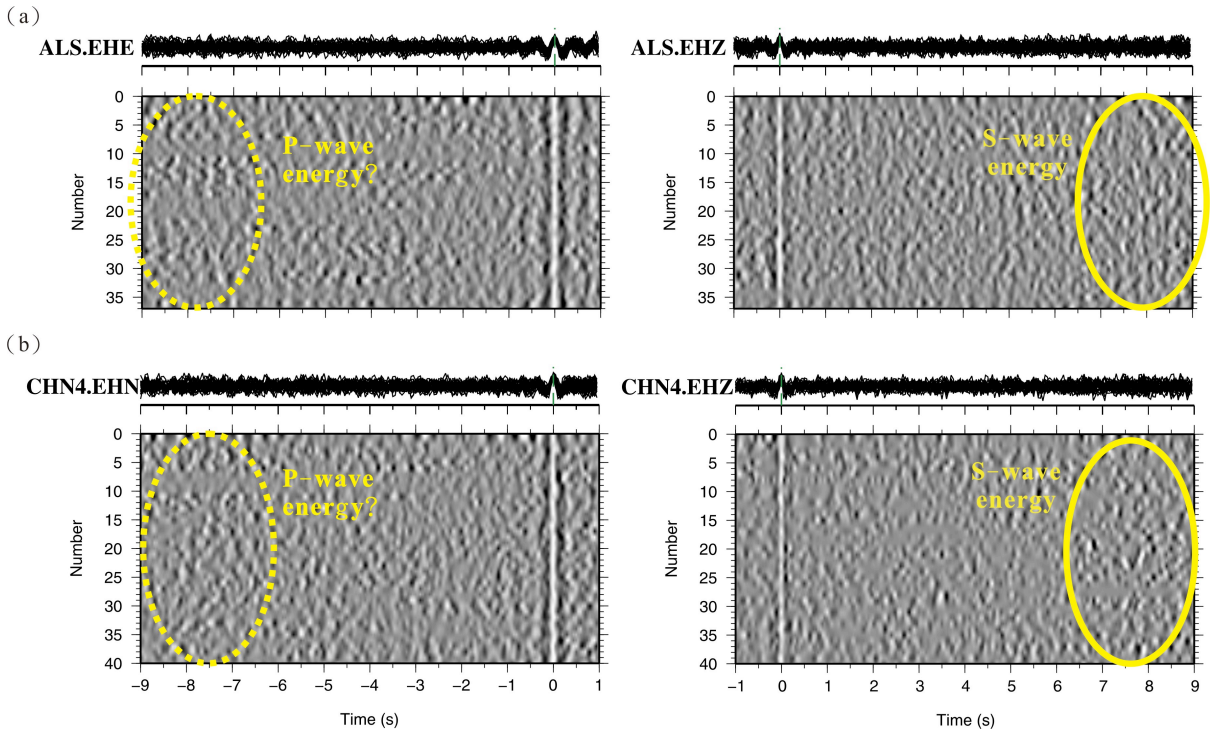

Figure S7. Alignment of *P*- and *S*-wave arrivals for stations **(a)** ALS and **(b)** CHN4 based on waveform cross correlation. Waveforms are amplitude normalized and band-pass-filtered between 2 and 8 Hz (black = -1 and white = +1 amplitude). A total of 10-s waveforms are plotted to show both the *P*- and *S*-wave arrivals. **(a)** In the left panel, clear *S*-wave phases are aligned on east-west component at 0 s. Some energy appears between -8.8 and -6.5 (yellow dot ellipse), which we infer as the *P*-wave energy. In right panel, a clear alignment of *P*-wave phases is shown on the vertical component and some *S*-wave energies appear between 6.5 and 8.8 seconds (yellow solid ellipse). **(b)** The same illustration for station CHN4. The range of *S*–*P* times is 6.1 ~ 8.6 s.

Figure S8.

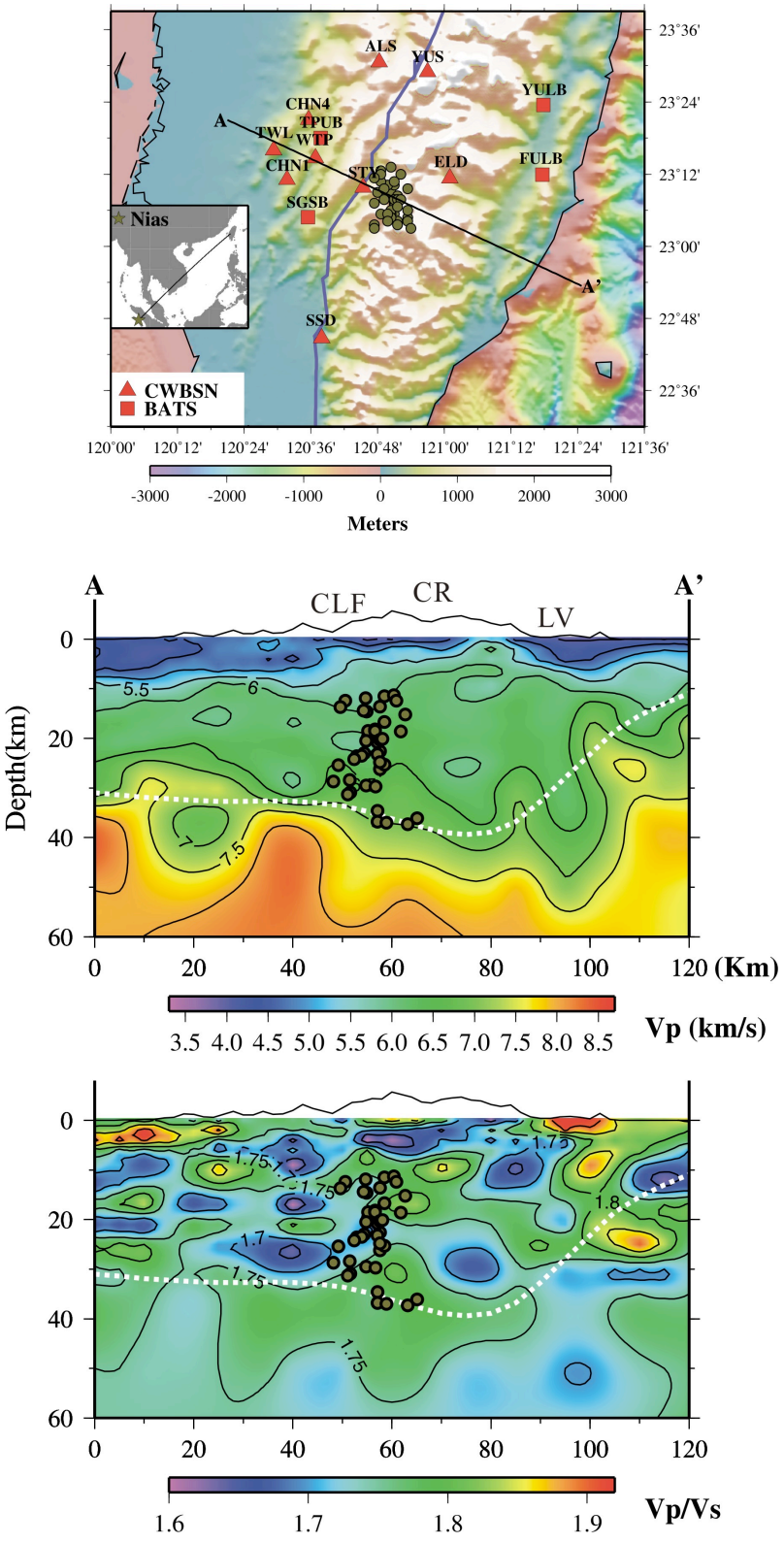

Figure S8. (a) The epicentral locations of the 41 LFEs based on the *Chen et al.* [2001] 1-D velocity model. The depth distribution of the 41 LFEs plotted on top of the 3-D Vp (b) and Vp/Vs model (c). Other symbols and notations are the same as in Figure 4.